IEEE Access
Multidisciplinary ⋮ Rapid Review ⋮ Open Access Journal

Received November 14, 2021, accepted November 30, 2021, date of publication December 3, 2021,
date of current version December 20, 2021.

Digital Object Identifier 10.1109/ACCESS.2021.3132775

An Adaptive Sequential Sampling Strategy-Based Multi-Objective Optimization of Aerodynamic Configuration for a Tandem-Wing UAV via a Surrogate Model

QINGLI SHI[1], HUA WANG[1], HAO CHENG[1], FENG CHENG[2], AND MENGLONG WANG[3]
[1]School of Astronautics, Beihang University, Beijing 100191, China
[2]China Academy of Launch Vehicle Technology, Beijing 100076, China
[3]Beijing Electro-Mechanical Engineering Institute, Beijing 100074, China

Corresponding author: Hao Cheng (chenghao_1030@buaa.edu.cn)

ABSTRACT Multi-objective optimization of aerodynamic configuration for a tandem-wing unmanned aerial vehicle (UAV) via a surrogate model is appropriate in the primary stages of aircraft design. This study presents an adaptive sequential sampling strategy, which takes into account the principle of entropy rank and selection pooling based on a sigmoid function (ESP), in order to save time and construct a surrogate model database with considerable approximation accuracy. The entire procedure of optimization is divided into four parts, involving problem formulation for design variables and objectives, database construction for the surrogate model, multi-objective optimization with the surrogate models, and ESP adaptive sequential sampling to update the database. Firstly, a comparative study of the different surrogate models is carried out to assess their approximation performance. This verifies that the radial basis function (RBF) surrogate model outperforms the other models across the board. Then, we conduct two tests with typical mathematical problems to validate the effectiveness and applicability of the proposed method. We also develop a multi-objective optimization of the aerodynamic configuration for a tandem-wing UAV, aiming to maximize the lifting coefficient at the ascent ($C_{Lascent}$) and the lift-drag ratio (K_{cruise}) during the cruise. In this case, the RBF surrogate model is proven more suitable than the other common methods to replace the real values calculated by the non-planar vortex-lattice method (VLM) during the process of optimization. Furthermore, a comparison with large minimal distance (LMD) sequential sampling and disposable Latin hypercube sampling (LHS) is carried out alongside the optimization. These results show that the approximation precision achieved using ESP strategy is greater, highlighting the superiority of the ESP adaptive sequential sampling strategy in reducing the number of samples and raising the approximation accuracy. Finally, after the refinement of the database, an optimal Pareto front set is obtained to guide the primary design of the aerodynamic configuration for the tandem-wing UAV. Then, it is verified that the selected trade-off optimal design point has a better aerodynamic performance than the initial reference point, improving $C_{Lascent}$ and K_{cruise} by 6.44% and 10.85%, respectively.

INDEX TERMS Aerodynamic configuration optimization, multi-objective, radial basis function, adaptive sequential sampling, entropy rank and selection pooling.

I. INTRODUCTION

Recently, tandem-wing UAVs have received widespread attention, because of advantageous aerodynamic configurations. Compared to aircrafts with conventional designs, a tandem-wing UAV has two pairs of airfoils situated at the fore and rear of the fuselage, which both generate considerable positive lift. This design balances aerodynamic and structural characteristics and the possibility of high maneuverability of the aircraft. A lot of research has focused on analysis of

The associate editor coordinating the review of this manuscript and approving it for publication was Hao Luo.

tandem-wing aerodynamic configurations [1]–[3]. Nevertheless, further research has found that there are influences on the aerodynamic characteristics for tandem-wing configurations. In order to investigate these interactions, two different methods, including tunnel experiments and numerical calculations, have been carried out for decades [4]–[7].

Wind tunnel experiments, being the most accurate way of calculating aerodynamics, have been conducted on a series of tandem-wing configurations. The results of these experiments confirmed the capacity of the total drag reduction and the lift increase by arranging the position between the fore and rear wings [8]. By contrast, numerical calculations of aerodynamics investigating tandem-wing configurations have also been carried out in the early stage of aircraft design, which has a financial and time cost advantage, although it offers slight loss of accuracy [9]–[11]. Cheng *et al.* investigated the unsteady aerodynamics in the morphing stage of a tandem-wing UAV by using the improved vortex lattice method. This research confirmed that the vortex-lattice method can accurately predict the unsteady aerodynamic performance [12]. Besides, the same team also proposed a method of predicting the lift coefficient of tandem-wing aircraft systems based on Prandtl's lifting-line theory [13]. The conclusions revealed the influence of some configuration variables acting alone on the performance of the aircraft systems.

However, it is more significant to focus attention on finding the optimum aerodynamic configuration of tandem-wing UAVs by considering all variables comprehensively. Due to the different performance requirements in each of the different flight stages, especially during ascent after take-off and during the cruising stage, the aerodynamic characteristics that have to be considered differ from each other. Therefore, optimization of a multiple-objective design problem needs to be discussed. The Non-Dominated Sorting Genetic Algorithm (NSGA-II) [14] has been proved effective to solve multi-objective optimization problems. It is considered more suitable than gradient based methods [15]–[17] used for the aerodynamic shape optimization (ASO) of the tandem-wing aircraft in this paper. As a kind of exploratory optimization method, NSGA-II considers the entire design space in the process of searching for the best configuration meaning that it is less prone to be trapped into the local optimum solution [18], [19].

The optimization procedure requires massive calculations for its multiple objectives and, as such, it is challenging to attain the corresponding aerodynamic characteristics by use of conventional methods such as tunnel experiments and numerical calculations, due to the time costs. In order to tackle this issue, numerical evaluation via a surrogate model has been applied in many studies, given it represents the real response of the characteristics with respect to design variables [20]–[24]. There are several kinds of surrogate models including deep neural networks (DNN) [25], radial basis functions (RBF), Kriging surrogate models (KRG), weighted average surrogates (WAS), and response surface

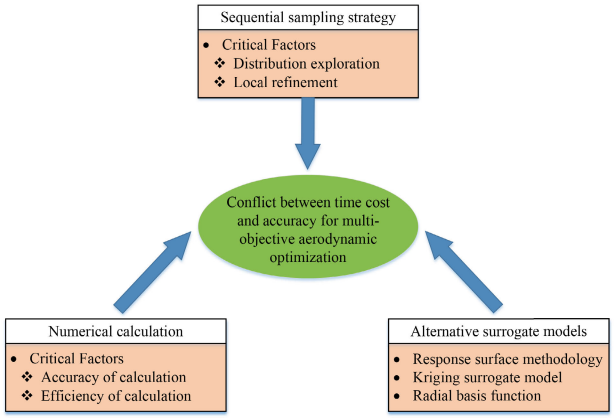

FIGURE 1. Technical challenge vs. alternative technical methods.

approximations (RSA), which have drawn intense attention in relevant fields [26]. The selection of the surrogate model used for the subsequent multi-objective optimization has a significant influence on the accuracy of the approximation. It is essential to take account of the general performance of different aspects including accuracy, robustness, and efficiency [27], especially for high dimension optimization cases. Additionally, to further reduce the total number of samples and ensure the precision of the surrogate model's approximation, a lot of effort has been made to add reasonable samples to a database based on infilling criteria [28]–[30]. Referring to a RBF power function and curvature sampling criteria, Huang *et al.* studied an improved adaptive criterion based on the root means square errors (RMSE) feedback and a crowdedness enhance function [31], showing broad prospects for the applications of aerodynamic optimization. However, most of the research into this strategy is not suitable for multi-objective optimization procedures, which have a requirement to balance the local refinement and the distribution exploration against two or more objectives with even contrary tendencies, during the optimization. Therefore, considering the challenges detailed above, in this paper we concentrated on establishing an efficient sampling strategy to accommodate multi-objective optimization.

Motivated by the above discussions, the conflict between the calculation time cost and accuracy is regarded as the primary challenge of multi-objective aerodynamic configuration optimization for tandem-wing aircrafts. Three critical alternative technical methods to solve the issues (sequential sampling strategy, numerical calculation, and surrogate models), accompanied by their key factors are shown in Fig. 1. In this study, we propose a novel ESP adaptive sequential sampling strategy to perform an aerodynamic configuration multi-objective optimization for a tandem-wing aircraft via a surrogate model. The main contributions are as follows:

(1) An adaptive sequential sampling strategy is proposed to update the database and require fewer samples with numerical simulation. Using this method, the entropy values are calculated based on the spatial distance to determine the rank of

each candidate, and a sigmoid function based on the entropy rank is used to help establish the final selection pooling. The infilling criterion comprehensively considers the capability of both the global and local searches. The entropy values of candidates show the uncertainty of points to be selected for updating the database and ensuring the exploration of the global distribution, and the selection pooling helps to jump out of the local optimum.

(2) Comparative simulations of three typical surrogate models are implemented, taking into account each model's efficiency, robustness, and accuracy. The results indicate that the RBF surrogate model is the most suitable for application to the multi-objective configuration optimization for tandem-wing aircraft. Based upon leave-one-out cross validation (LOOCV), we propose a novel optimization method for the shape parameters of surrogate models with parallel calculation, which effectively improves the approximation accuracy.

(3) In order to further reduce the time costs of the entire optimization process, the non-planar VLM method (instead of the conventional numerical calculation method) is utilized to calculate the aerodynamic performance. We can then validate that the errors between two numerical simulations are narrowed into a small margin.

II. MULTI-OBJECTIVE OPTIMIZATION PROCEDURE

Figure 2 illustrates the multi-objective optimization process for aerodynamic configuration, which is used in this paper. Firstly, the formulation of the problem is developed, which considers two aerodynamic characteristics as optimization objectives and five parametrization variables in terms of the position distribution and wingspan between the fore and rear wings of a tandem-wing UAV. Then, initial design points are obtained by the design of experiment (DOE) using Latin Hypercube Sampling (LHS) [32], which covers the whole design space S and fits the nonlinear response effectively. After the design of experiment, the mesh generation and numerical calculations are implemented to evaluate the aerodynamic performance. The results are stored in the incipient database, followed by construction of the surrogate model to approximate the objectives corresponding to the design variables, and the NSGA-II method is applied in order for optimization. However, due to differences between the RBF approximation and the numerical simulation, it is hard to achieve the real Pareto-optimal Front (PoF). An adaptive sequential sampling method to enlarge the training database is used to eliminate approximation errors. Finally, another iteration is carried out from the step of the RBF evaluation construction and employing the updated database, until the gaps of both objectives converge to a certain precision.

A. PROBLEM FORMULATION AND CONFIGURATION PARAMETRIZATION

In this study, the tandem-wing configuration UAV including fuselage is described in the body coordinate system $OX_bY_bZ_b$, as demonstrated in Fig. 3. The differences in aerodynamic

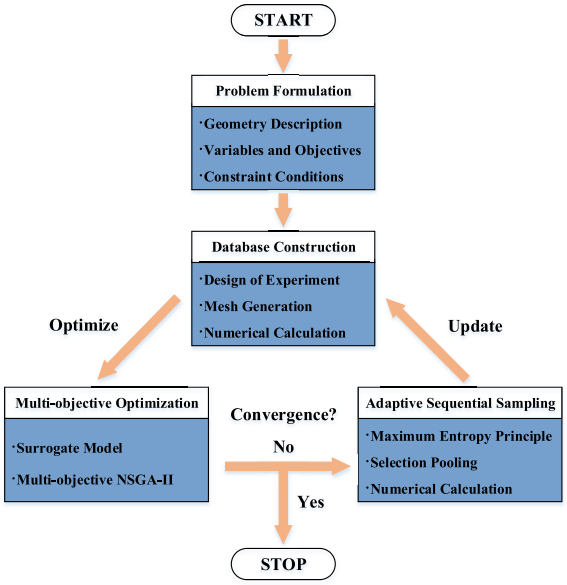

FIGURE 2. Flowchart of multi-objective optimization strategy for aerodynamic configuration.

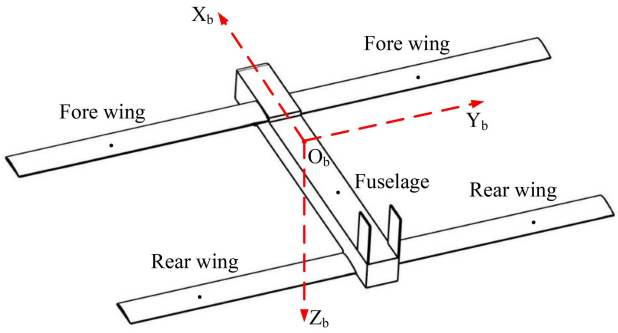

FIGURE 3. Body coordinate system.

characteristics for tandem-wing aircraft are primarily influenced by the aerodynamic interaction between the two pairs of wings, with little relationship of the fuselage and especially at a low angle-of-attack. This was verified with computational fluid dynamics (CFD) and use of the lifting line method by Cheng and Wang [13]. Five design variables are considered from the aspect of the three-dimensional position distribution between fore and rear wings and the wingspans of the two pairs of wings, as shown in Fig. 4. Firstly, *Stagger* and *Gap* represent the vertical distance and the horizontal distance of the two lifting surfaces respectively, expressed as S_t and G. Meanwhile, the difference in the relative span length ratios between the two pairs of wings $r_b = b_1/b_2$ (b_1 for span length of the fore wings and b_2 for span length of the rear wings) brings different aerodynamic characteristics. This is owing to the area variation of the fore wings' downwash effect on the rear wings and the rear wings' upwash effect on the fore wings. Moreover, reasonable selecting of the incidences of the two wings τ_1, and τ_2 can also adjust the downwash and upwash effects.

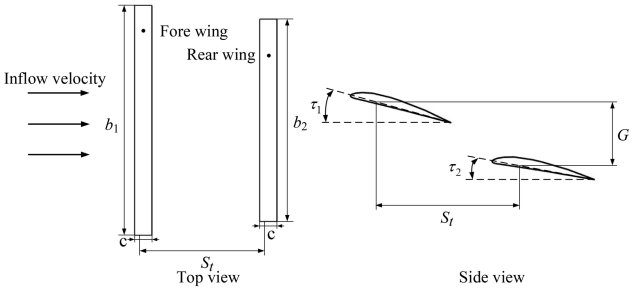

FIGURE 4. Aerodynamic configuration described from two aspects.

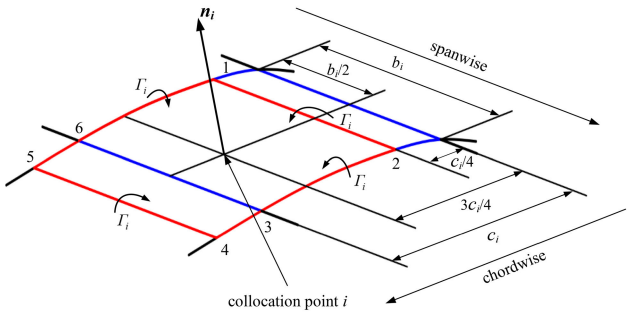

FIGURE 5. Constitute and direction of a single vortex ring.

TABLE 1. Design space.

design variables	Type	range
S_t	Continuous	$(6c - 8c)$
G	Continuous	$(-0.9c - 0.9c)$
r_b	Continuous	$(0.82 - 1.50)$
$\tau_1/(^\circ)$	Continuous	$(0 - 2.5)$
$\tau_2/(^\circ)$	Continuous	$(0 - 2.5)$

The ranges of design variables are listed in Table 1, which is suitable to balance between generations for high quality pneumatic profiles and limitations on folding requirements. In this table, c is the chord of both the two pairs of wings.

In addition, a constraint is proposed in that the total reference area of the two wings S_{total} is restricted to a constant for calculation of the aerodynamic coefficients.

By aiming to optimize the aerodynamic configuration of the tandem-wing UAV, attention is drawn to the aerodynamic characteristics of different cases. Two typical objectives are discussed in this paper. The first one is the lift coefficient C_L at a specific angle of attack ($\alpha = 3^\circ$) during the ascent stage and secondly, the lift-drag ratio $K = C_L/C_D$ under cruise design points with a constant lift coefficient ($C_L = 0.5$). In this way, the flight performance envelope, where the velocity is set as $v = 30m/s$ at a low altitude, can be satisfied.

B. DATABASE CONSTRUCTION BASED UPON NUMERICAL CALCULATION

1) DESIGN OF EXPERIMENT

In this paper, a set of design points, selected by the design of experiment technique as training samples, is employed to construct the initial database for the surrogate model. This consists of a group of design variables $X^i = (S_t^i, G^i, r_b^i, \tau_1^i, \tau_2^i)$ and two objective functions $Y^i = (C_L^i, K^i)$. In the M-dimension space, LHS divides each design variables X_j ($j \in [1, M]$) into N intervals of equal probability, and each interval is sampled once at a random order. Then, a $M \times N$ coupling LHS is constructed [33]. To uniformly discretize the design space, and achieve the most precise, but least number of training samples for the meta model, the values of each design variables' dimensions can be combined casually.

2) MESH GENERATION AND NUMERICAL CALCULATION

In this study, a conflict exists between precision and efficiency of the calculation of aerodynamic characteristics for the tandem-wing aircrafts, especially in the process of optimization where there are masses of iterations. The high fidelity numerical simulation method, computational fluid dynamics (CFD), has been commonly employed but with a high computational time cost. Recently, the non-planar VLM has been gradually applied as a helpful numerical calculation method, which can lead to an expeditious and accurate aerodynamic design and optimization procedure, due to the fact that it has a lower computational time cost than that of the CFD method.

Taking into account the camber of aerofoil, the non-planar VLM method discretizes the center camber surface of wings to generate a series of mesh surfaces with the horseshoe vortexes replaced by vortex rings attached to each mesh surface. Each vortex ring consists of six vortex segments, of which the leading vortex segment is placed at the quarter chord line of the mesh element, and the tailing vortex segment is aligned with the quarter chord line of the next downstream mesh element. The other four segments connect the line from the tailing edge point of the mesh element, to the leading vortex segment and the tailing vortex segment, coinciding with both side boundaries of the mesh element. The collocation point is located at the three-quarter chord line of the mesh element's center symmetry, of which the normal direction determines that of the mesh element. The schematic diagram of a single vortex ring is shown in Fig. 5.

Meanwhile, horseshoe wake vortices extend behind the mesh of the wing trailing edge, simulating the surface effect more accurately. The direction of wake vortices are the same as that of the freestream velocity, and the magnitude of the vortex ring is equal to that of the trailing edge vortices of the adjacent upstream vortex ring. The schematic diagram, Fig. 6 shows the distribution of vortex rings in the non-planar VLM for the tandem-wing configuration.

According to Biot-Savart Law, the induced velocities generated by each vortex segment can be obtained as follows

$$V = \frac{\Gamma}{4\pi} \frac{r_1 \times r_2}{|r_1 \times r_2|^2} \left[r_0 \cdot \left(\frac{r_1}{|r_1|} - \frac{r_2}{|r_2|} \right) \right] \tag{1}$$

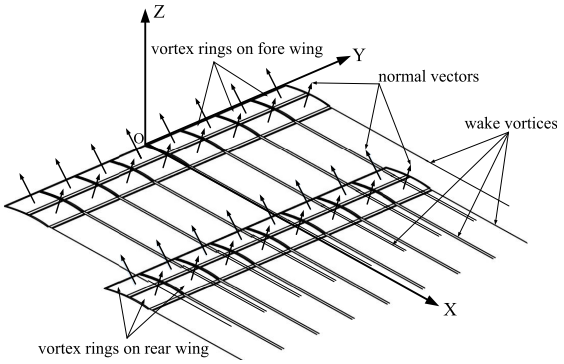

FIGURE 6. The distribution of vortex rings in the non-planar VLM for the tandem-wing configuration.

where Γ represents the vortex intensity, r_1 and r_2 represent the spatial vector from the starting point and the ending point of each vortex segment, to the collocation points, and r_0 represents the vector from the starting point to the ending point of the vortex segment.

Next, the total induced velocity V_{ij} generated by the jth vortex ring at collocation i can be derived as the resultant velocity of the induced velocities generated by all six segments of the jth vortex ring.

$$V_{ij} = \Gamma_j v_{ij} = \Gamma_j (v_{ij12} + v_{ij23} + v_{ij34} + v_{ij45} + v_{ij56} + v_{ij61}) \tag{2}$$

where v_{ij} represents the induced velocity at collocation i generated by jth vortex ring with the unit vortex intensity.

On the other hand, based on the fact that the intensity of the wake vortex is equal to that of the trailing vortex of the upstream mesh element, the induced velocities generated by the vortex rings near the tailing edge of the lifting surfaces can be calculated by the computational formula for horseshoe vortices, which is expressed as

$$\begin{aligned} V = & \frac{\Gamma}{4\pi} \frac{V_\infty \times r_2}{|r_2|(|r_2| - V_\infty \cdot r_2)} \\ & + \frac{\Gamma}{4\pi} \frac{(|r_1| + |r_2|)(r_1 \times r_2)}{|r_1||r_2|(|r_1||r_2| + r_1 \cdot r_2)} \\ & - \frac{\Gamma}{4\pi} \frac{V_\infty \times r_1}{|r_1|(|r_1| - V_\infty \cdot r_1)} \end{aligned} \tag{3}$$

where V_∞ represents the vector of the freestream velocity.

According to the Neumann boundary condition, which means that the flow cannot go through the center camber surface at the collocation point, the local velocity should be orthogonal to the normal vector of the corresponding collocation point. This is expressed as

$$\left(V_\infty + \sum_{j=1}^{n_p} \Gamma_j v_{ij}\right) \cdot n_i = 0. \tag{4}$$

By applying (4) at all collocation points of the two wings on the tandem-wing aircraft, a linear system of equations can be obtained.

$$[A]\{\Gamma\} = B \tag{5}$$

where,

$$[A] = \begin{bmatrix} v_{11} \cdot n_1 & \cdots & v_{1n_p} \cdot n_1 \\ v_{21} \cdot n_2 & \cdots & v_{2n_p} \cdot n_2 \\ \vdots & \ddots & \vdots \\ v_{n_p1} \cdot n_{n_p} & \ldots & v_{n_pn_p} \cdot n_{n_p} \end{bmatrix} \tag{6}$$

$$\{\Gamma\} = [\Gamma_1, \Gamma_2, \cdots, \Gamma_{n_p}]^T \tag{7}$$

$$\{B\} = [-V_\infty \cdot n_1, -V_\infty \cdot n_2, \cdots, -V_\infty \cdot n_{n_p}]^T \tag{8}$$

where $n_p = 2N$ is the number of collocation points.

By solving the linear system of equations above, the intensity of each vortex ring can be obtained. According to the Kutta-Joukowski Theroem, the forces acting on each mesh element are derived as

$$\begin{aligned} F_i = & \rho(\Gamma_i - \Gamma_U)V_i \times l_{12} + \rho(\Gamma_i - \Gamma_R)V_i \times l_{23} \\ & + \rho(\Gamma_U - \Gamma_{UR})V_i \times l_{34} + \rho(\Gamma_U - \Gamma_{UL})V_i \times l_{56} \\ & + \rho(\Gamma_i - \Gamma_L)V_i \times l_{61} \end{aligned} \tag{9}$$

where $\Gamma_i, \Gamma_U, \Gamma_L, \Gamma_R, \Gamma_{UL}$, and Γ_{UR} represent the intensities of the current mesh vortex ring, the upstream mesh vortex ring, the left mesh vortex ring, the right mesh vortex ring, the upstream left mesh vortex ring, and the upstream right mesh vortex ring, respectively. $l_{12}, l_{23}, l_{34}, l_{56}, l_{61}$ represent the vector from starting points to ending points of each corresponding segment of the current mesh element, and V_i represents the resultant velocity vector at the current mesh collocation point.

Then, the vector of the aerodynamic force can be decomposed into the lift and the induced drag, which can be expressed as

$$\begin{cases} L = \sum_{j=1}^{2N} F_j \cdot u_l \\ D = \sum_{j=1}^{2N} F_j \cdot u_d \end{cases} \tag{10}$$

where $u_l = [-\sin\alpha, \cos\alpha, 0]^T$ and $u_d = [\cos\alpha, \sin\alpha, 0]^T$ represent the unit vector in the lift direction and induced drag direction, and α is the angle of attack.

3) VALIDATION OF THE NUMERICAL CALCULATION METHOD

In the present study, a lot of research implemented the flow solution validation method based on numerical calculations for aerodynamic characteristics of aircrafts [34]–[36]. Xie *et al.* validated the aerodynamic characteristics obtained by using non-planar VLM compared against the experimental data from the wind tunnel tests [37]. Our previous comparative work, which used CFD method, adequately validated the accuracy and capability of non-linear VLM when calculating aerodynamic characteristics for tandem-wing aircraft [11], [12]. The results are shown in Fig. 7. It was indicated that non-planar VLM had acceptable calculation accuracy, which was in agreement with the test results of the

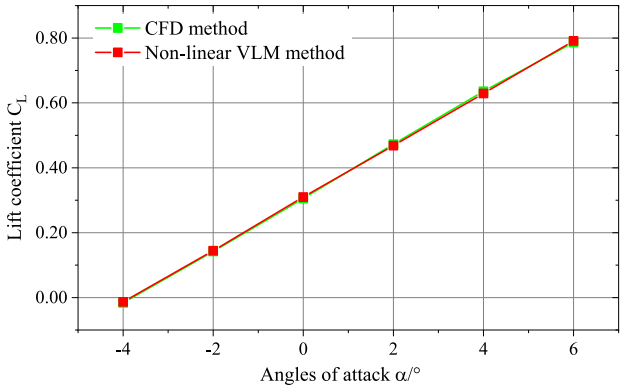

FIGURE 7. The calculation accuracy of non-linear VLM compared with CFD.

TABLE 2. Mesh independency analysis strategy.

Mesh elements		
spanwise	chordwise	total
17	4, 10, 20, 30, 40, 50	68~850
chordwise	spanwise	total
40	1, 5, 9, 13, 17, 21	40~840

CFD method. On the other hand, the balance between the computational efficiency and accuracy of non-planar VLM indicates that it is suitable to be applied in the preliminary design stage, as well as detailed design stage, of aircraft.

Mesh independence analysis is necessary to approximate aerodynamic performance using the numerical calculation method. Two crucial parameters of the mesh element for non-planar VLM, involves the number of mesh elements along the span wise direction and chord wise direction respectively, explicitly shown in Table 2. Meanwhile, the variation of the attack angles to be verified range from -2° to 4°. The results of the mesh independence analysis are demonstrated in Fig. 8. It is indicated that, as the angle of attack increases, the lift coefficient and the induced drag coefficient both tend to stabilize gradually with the refining of the mesh along the two directions. For the sake of the time cost, a combination of mesh element numbers along the two directions $N_b = 40, N_c = 17$ are selected, in the meantime, to consider the accuracy of the simulation.

C. SURROGATE-MODELING TECHNIQUES

During the multi-objective optimization process, there are abundant calculations of the objective functions. Numerical simulation poses an expensive time cost, which significantly influences the optimization efficiency. Instead of performing costly numerical simulations, a surrogate model can be used to evaluate the real functions. Many scholars have researched different surrogate techniques [38]–[40]. These methods seem to be advantageous in certain instances but still struggle to perform well in others. In this study, we introduced common surrogate-model methods, including response

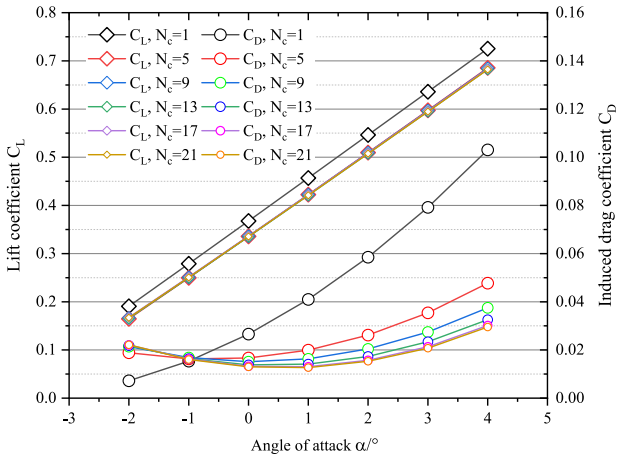

(a) Along chordwise direction (N_b = 40).

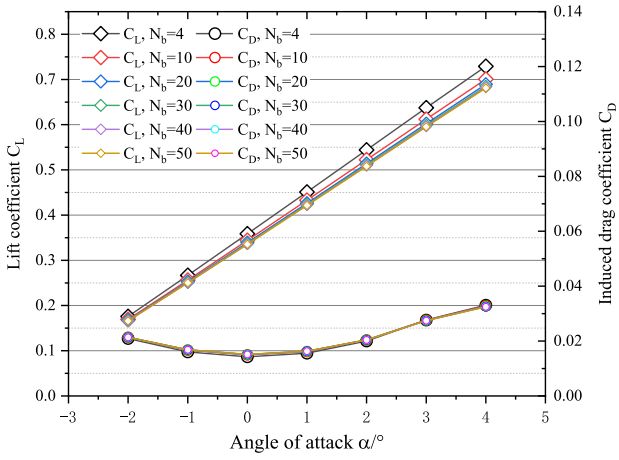

(b) Along spanwise direction (N_c = 17).

FIGURE 8. Mesh independence analysis.

surface methodology (RSM), the Kriging model (KRG), and the radial basis function model (RBF).

1) RESPONSE SURFACE METHODOLOGY

The response surface methodology (RSM) employs a statistical regression technique by fitting a simple polynomial to the responses obtained from simulations or experiments. The response surface model can be expressed as a general form:

$$f_k = \beta_0 + \sum_{i=1}^{Nv} \beta_i X_i + \sum_{i=1}^{Nv} \sum_{j=1}^{Nv} \beta_{ij} X_i X_j + \sum_{i=1}^{Nv} \beta_{ii} X_i^2 \quad (11)$$

where f_k represents the response of unknown functions, and X_i, X_j represent the design variables. Nv is the number of design variables, and β_0, β_i, β_{ij}, and β_{ii} are the regression coefficients for the constant, linear, intersection, and square terms, respectively. Based on the least square method, the vector β can be derived as follows:

$$\beta = (X^T X)^{-1} X^T Y \quad (12)$$

where Y is the real values of functions to be estimated, and X is the GRAMIAN matrix related to the number of design variables and the order of the polynomial response surface. It is observed that RSM has the advantage of constructing an approximation model simply and quickly, but it is not suitable for solving problems that are highly non-linear.

2) KRIGING SURROGATE MODEL

The Kriging surrogate model correlates related information of unknown spatial objectives with known spatial samples. In essence, it is an improvement of the regression algorithm, which employs covariance to measure the degree of spatial correlation at each sample point, including linear regression and variation function. For an expensive function $y = f(x)$, $x \in \Re^n$, the predictor $\hat{y}$ is defined as:

$$\hat{y} = \alpha(x) + \beta(x) \tag{13}$$

where $\alpha(x)$ is the regression model, and $\beta(x)$ shows a stochastic process with an assumption of the following covariance:

$$Cov[b(x^i), b(x^j)] = \sigma^2 R(\theta, x^i, x^j) \tag{14}$$

where $R(\theta, x^i, x^j)$ is the spatial correlation function with parameters θ, and σ is the standard deviation.

Alternative types of correlation models involve Linear, Spherical, Cubic, Spline, and Gaussian methods, in which Gaussian is the most commonly used in the Kriging surrogate model.

3) RADIAL BASIS FUNCTION

Radial basis function (RBF) is a surrogate model with a linear combination of basis functions. For the database (X^i, Y_j^i) $(j = 1, 2, \cdots, m)$ in the real-value space $\Re^n$, the RBF interpolation model can be constructed as follows:

$$\hat{f} = \sum_{i=1}^{n} \alpha_i \phi(\|x - x^i\|), \quad x \in \Re^n \tag{15}$$

where m is the number of the objectives; n is the total number of sample points and $\|\cdot\|$ is the Euclidean norm. In a linear system $A\alpha = f$ with a symmetric matrix $A_{ij} = \phi(\|x - x^i\|)$ and $f = [Y_j^1, Y_j^2, \cdots, Y_j^n]^T$ $(j = 1, 2, \cdots, m)$ for each objective, the coefficients $\alpha = [\alpha_1, \alpha_2, \cdots, \alpha_n]^T$ are produced by the interpolation conditions. A univariate continuous radial basis function ϕ includes many forms, such as the multi-quadric function $\phi(r) = 1/\sqrt{r^2 + c^2}$ and the Gaussian radial function $\phi(r) = e^{-c^2 r^2}$, whereby c is the shape parameter of the RBF model.

4) PARAMETER OPTIMIZATION FOR SURROGATE MODELS

In order to choose an adequate surrogate model for use during the process of multi-objective optimization, a series of comparative simulations were implemented to explore the performance of the three different surrogate models: the response surface methodology, the Kriging model, and the radial basis function model. It is necessary for the KRG and RBF surrogate models to have a proper value selection for the shape parameter c and the initial parameter θ_0. In order to be highly accurate, the RBF and KRG models depend on the number and the distribution of the data points, the data response, and the accuracy of the calculation [41]. It is more accurate and adaptable to optimize the shape parameter, compared with choosing a constant value. To evaluate the adequate shape parameters and the initial parameters for various problems, a leave-one-out cross validation (LOOCV) method was applied, without additional function evaluations. For each step i in the process, all the points except X^i, which served as the test point, were used to construct a RBF or KRG surrogate model, and the resulting errors between the approximation values and the actual ones are termed to be LOO errors. After a loop of every sample point tested, an indicator RMSE was obtained, which can be expressed as

$$RMSE = \frac{\sqrt{\frac{1}{n}\sum_{i=1}^{n}(f_i - \hat{f}_i)^2}}{\frac{1}{n}\sum_{i=1}^{n}|f_i|} \tag{16}$$

where f_i are the actual values and $\hat{f}_i$ are the estimated values.

Taking the optimization process of the shape parameter for the RBF surrogate model based on LOOCV as an example, a nonuniform shape parameter, randomly based on the selecting strategy for different sample points was proposed as follows [42],

$$c_i = c_{opt} \times [1.0 + \text{rand}_i(-1.0, 1.0) \times \beta] \quad (i = 1, 2, \ldots, It_{max}) \tag{17}$$

where It_{max} is the maximum number of iterations, $\beta = 0.1$ is a constant random coefficient, and c_{opt} represents the optimal value of the shape parameter at the current optimization step with the minimum of RMSE as the single objective. Then, the new parameter c_i is generated for construction of the RBF model and the c_{opt} is updated via a comparison between c_i and c_{opt} at the last iteration. In addition, the adaptive random search coefficient β in Equation (17) is expressed as

$$\beta = 0.05 + 0.25 \times \frac{Max - i}{Max}, \quad i = 1, 2, \ldots, Max \tag{18}$$

where Max is the maximum iterations. It ensures both search speed at the initial phase and convergence precision in the last stage.

The method above shows great accuracy and effectiveness of approximation without much of an increase in complexity and computational cost [42]. However, the simple optimization structure may cause trapping in the local optimum and insufficient searching precision. In order to enhance the global search performance of the non-uniform search strategy in all aspects, this paper employs a method of parallel computing with an adaptive random search coefficient. The best optimization solution can be chosen from multiple obtained solutions. The method effectively decreases the probability of falling into the local optimum, where the number of parallels corresponds to the number of computer cores.

Likewise, the optimization of the initial parameter for the Kriging model is developed in similar process.

5) COMPARISON OF DIFFERENT SURROGATE MODELS

In order to comprehensively test the performance of the three different surrogate models, we performed comparative studies composing of a series of multi-objective functions with the same mathematical structure (e.g. FONT [43]) as the standard reference value for the surrogate approximation. The expression of the test function is as follows. As is illustrated, with step-by-step iterations of the training database update, both the RMSE with the KRG and RBF surrogate models decrease gradually, but the RMSE with the RSM surrogate model develop no obvious downward trend.

$$\text{FONT}: \begin{cases} f_1(x) = 1 - \exp(-\sum_{i=1}^{m}(x_i - 1/\sqrt{m})^2) \\ f_2(x) = 1 - \exp(-\sum_{i=1}^{m}(x_i + 1/\sqrt{m})^2) \end{cases} \quad x_i \in [0, 1] \tag{19}$$

where m is the number of design variables.

In this part of the study, a training database with 100 data lines was using the Latin Hypercube method, so that three surrogate models would not perform poorly, especially in the high-dimensional test problems. Then, three typical performance index, including accuracy, robustness, and efficiency, were used to assess the quality of the different surrogate models. Below, we describe the evaluation criteria in detail.

The accuracy is the capability of the approximation to get close to the real values, which can be measured with R^2, expressed as

$$R^2 = 1 - \frac{\sum_{i=1}^{N}(f_i - \hat{f}_i)^2}{\sum_{i=1}^{N}(f_i - \bar{f}_i)^2} \tag{20}$$

where N is the number of training samples, f_i is the actual value, $\hat{f}_i$ is the estimated value, and $\bar{f}_i$ is the averaged actual value.

The robustness refers to the capability of the surrogate models to retain a consistent level of accuracy across differing problems. Consequently, in this work, the design variable number of the alterable test problems ranged from 3 to 10 with a controlled interval, and the prediction accuracy of each case was calculated to achieve the average behaviors.

The efficiency represents the calculation effort in constructing the surrogate models and approximating a new response. In this work, the efficiency of each surrogate model was measured according to the time cost for establishing the surrogate model with a size of 100 and predicting a set of new input points with a size of 1000.

The results of these comparative approximations, with different surrogate models are as follows. Fig. 9 shows the variations of the R^2-metric to the approximation values obtained by RSM, KRG, and RBF respectively, with a design variable number v=[3,5,7,9,10]. It is apparent that the accuracy of RBF is higher than the other two models and that the precision of RSM is the worst, no matter which design variable number. Additionally, according to the accuracy calculation results for the two-objective function *FONT*, the RBF surrogate model performs steadily and is strongly robust, despite a slight decrease in the accuracy as the design variable number increases. By contrast, the other models both have sharp declines in their accuracy performance. On the other hand, Table 3 lists the time taken to calculate each of the prediction sets, which adequately demonstrates the RBF surrogate model's advantage of computational efficiency.

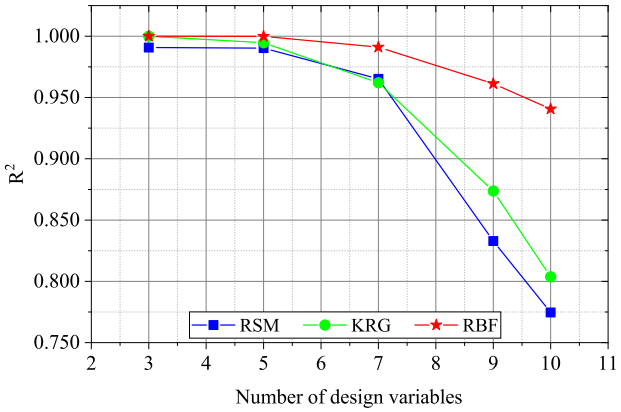

(a) Variations for objective F1.

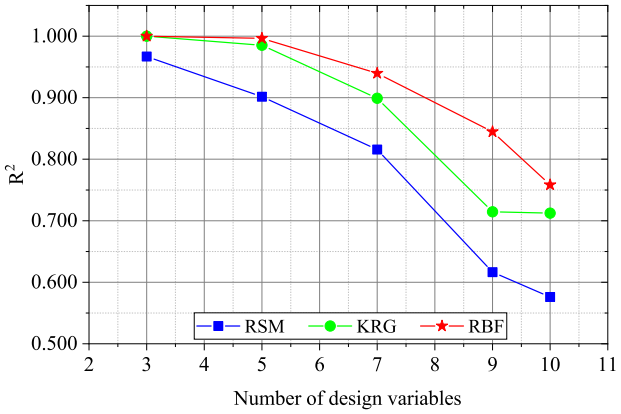

(b) Variations for objective F2.

FIGURE 9. The variations of the R^2-metric to the approximation values by different surrogate models for the multi-objective function.

TABLE 3. Comparison in computing efficiency with different surrogate models.

surrogate models	calculation time
RSM	0.1351s
KRG	0.1181s
RBF	0.0534s

D. MULTI-OBJECTIVE OPTIMIZATION BASED ON NSGA-II

In this paper, the goal was to perform a multi-objective optimization of the aerodynamic shape of a tandem-wing UAV, which depends on the selection of the optimal search method. The non-dominated sorting genetic algorithm NSGA-II [44] has been widely used in the academic community all over the world, and has been shown to outperform other methods. NSGA-II has no difficulty in maintaining a wide spread of solutions over the achieved Pareto-optimal Front, based upon

a rank and crowded comparison strategy. It can also reduce the computation cost but retain a high degree of accuracy by using a method of fast non-dominated sorting [14].

E. ADAPTIVE SEQUENTIAL SAMPLING STRATEGY

It is usually difficult for researchers to attain an adequate number of samples in the initial stages, which has a significant influence on the precision of optimization. Fewer design points may cause a large gap away from the real Pareto-optimal Front, but a high number of samples require a big computational cost without an advantage or obvious increase in the calculation accuracy. Therefore, this study proposed an ESP adaptive sequential sampling strategy to solve this contradiction.

To begin with, an initial sample distribution based on the LHS and with an empirical size of $v\times(v+1)$ was implemented (v=design variables), which usually produces widely deviating results in most optimization problems. A crude RBF approximation model was built using these initial sample points to perform the multi-objective optimization. Then, additional training samples were chosen in the design space according to a certain sampling criterion, and a non-VLM numerical calculation was carried out before updating the database. The loops of this process did not stop until the optimized results converged to a specified precision. Thus, two essential factors (local refinement and distribution exploration) in the adaptive sequential sampling procedure determined the performance of the multi-objective optimization, which had to maintain a balance between themselves.

In order to balance local refinement and distribution exploration, we proposed an adaptive local incremental sampling method, based on the strategies of increasing entropy and selection pooling (ESP). This attempted to avoid a disordered searching process for the optimal adding points. 'Entropy' as a chemical terminology is used to describe the perplexity of a system. As the entropy increased, the degree of chaos in the system kept rising. In this paper, an entropy was defined to represent the uncertainty in the set of points to be selected for updating the training samples. Each of the m points in the candidate set had an Euclidean distance from the n current training sample points. Accordingly the object property matrix $D=(d_{ij})_{m\times n}$ is expressed as follows

$$D=\begin{pmatrix} d_{11} & \cdots & d_{1n} \\ \vdots & \ddots & \vdots \\ d_{m1} & \cdots & d_{mn} \end{pmatrix} \tag{21}$$

where d_{ij} is regarded as the Euclidean distance between the ith candidate point and the jth training point. Then, in this $m\times n$ system, the entropy of the ith candidate point is defined as

$$H_i=-k\sum_{j=1}^{n} f_{ij}\ln f_{ij},\quad i=1,2,\cdots,m \tag{22}$$

where $k=1/\ln n$ and $f_{ij}=d_{ij}/\sum_{j=1}^{n} d_{ij}$. In this way, the distribution exploration is achieved by selecting the additional points according to the order of entropy. The large value represents high uncertainty within the system, which means there is a low degree of accuracy in predicting the corresponding domain.

Nevertheless, it is also important to maintain the global diversity of the system at the same time as ensuring its global precision. We implemented an adaptive local incremental selection approach based on the entropy calculated above. In this study, a sigmoid function [45] was defined to assign the disturbance number of the individual in sparse areas. In this study, there was a selection pooling with a scale of S_{max}, consisting of the candidate points alongside their duplicates, and constructed using the sigmoid function with a non-linear property. Where the function variable was the entropy value mentioned above, this selected more additional reasonable points for addition to the database to construct surrogate models. After a process of entropy normalization, the sigmoid function could be expressed as follows

$$y=\begin{cases} (uh-1)(2h^2+\dfrac{1}{uh-1}) & 0\le h\le 0.5 \\ (uh-1)(1-2(h-1)^2+\dfrac{1}{uh-1}) & 0.5\le h\le 1 \end{cases} \tag{23}$$

where h is the normalized entropy, and uh is the maximum clone value. Fig. 10 shows the variation trend of the clone values y with different normalized entropy values. Then, to construct the selection pooling, the duplicate number of each candidate Dup is defined as $Dup=floor(y)$. On the other hand, as far as local refinement is concerned, it was beneficial to choose the current Pareto front points as the candidate set, which extended the local optimum character during the optimization process and enhanced the probability of approaching the real PoF. Furthermore, in order to avoid becoming trapped in the local optimum solution, each of elements in the selection pooling was seen as a center around an adequate ε neighborhood of themselves, of which the radius is expressed as

$$R=\mu d_{min} \tag{24}$$

where μ is a scaling factor, and d_{min} represents the minimum distance between the candidate points and the training samples. Then, the final adding sample is a certain point in the neighborhood of the selected center.

III. TESTABILITY VERIFICATION WITH A MATHEMATICAL PROBLEM

In this paper, two tests with a typical mathematical problem such as FONT were carried out in order to evaluate the applicability, effectiveness and superiority of the RBF surrogate model combined with the adaptive sequential sampling strategy for multi-objective optimization, whilst maintaining a balance between distribution exploration and local refinement. The expression of the test problem is shown as Eq. (19).

In the first test, the three surrogate models (RSM, KRG and RBF) were used as alternatives for calculating the real values of the test functions, during the process of the

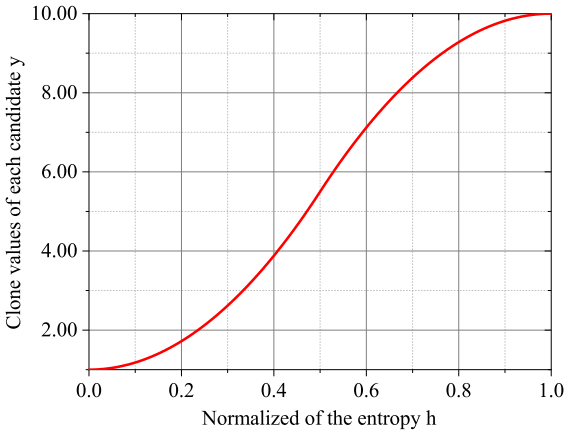

FIGURE 10. The variation trend of the clone values *y* with the sigmoid function.

multi-objective optimization and based upon the ESP sequential sampling method. In this case, five design variables were decided, and the LHS method was used to produce the initial training database with 30 data lines. By running the search with uses of the optimization algorithm NSGA-II, the initial population was set to 100 with a maximal evolution number of 400. The parameters of cross recombination and mutation probabilities were 0.9 and 0.1. Then, after 60 iterations of updating different surrogate models, three groups of results were obtained. Also, relative errors, denoted by RMSE of training samples with LOOCV method, were monitored as an evaluation index of each model, as shown in Fig. 11.

As it is illustrated, with step-by-step iterations of the training database updated, the RMSE with both the KRG and RBF surrogate models decreased gradually, but the RMSE with the RSM surrogate model developed no obvious downward trend. Comparing the RMSE convergence of two arithmetic cases with the KRG and RBF surrogate models, suggests that the RBF surrogate model performs better than the KRG model in terms of accuracy, especially for the first objective. The RMSE values of the first objective RBF estimation decrease from 5.22% to 0.22% by adding 60 reasonably selected points to the 30 samples originally selected. The corresponding values for the KRG surrogate model just reached 0.78%. Therefore, it is shown that the RBF surrogate model is the most effective and suitable for the multi-objective optimization procedures described in this work.

In the other test, according to the validation results obtained above, the RBF surrogate model with the superiority on accuracy and efficiency was chosen for application to a performance comparison between the proposed adaptive ESP sequential sampling strategy and a previous largest minimum distance (LMD) method. Fig. 12 illustrates the RMSE convergence trends of two-objective functions with different training sample infilling criterion. Meanwhile, the RMSE of disposable Latin hypercube sampling was contained as a benchmark to show the efficiency of the sampling strategy proposed above. In Fig. 12, it is obvious that

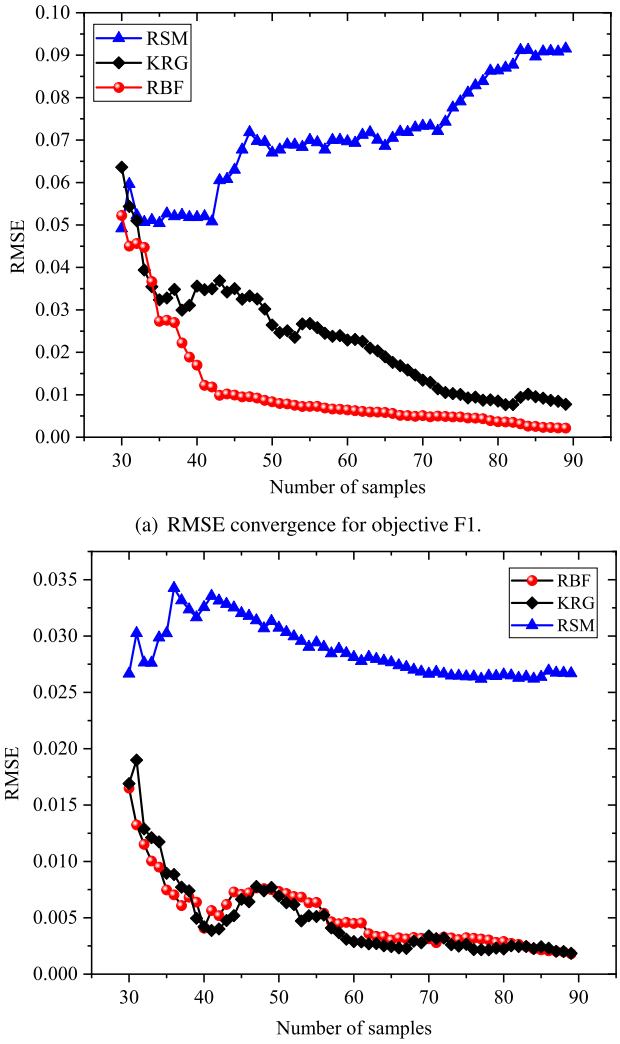

(a) RMSE convergence for objective F1.

(b) RMSE convergence for objective F2.

FIGURE 11. RMSE convergence of the two-objective function with different surrogate models.

approximation precisions with both sequential sampling methods were almost larger than the benchmark, especially for the first objective. Nevertheless, the RMSE values appeared to be on the decline gradually to the target after adding more refinement samples. If RMSE= [0.011, 0.0061] is taken as the benchmark, the LHS method needed to increase [40,40] samples and LMD sampling method needed to add [30,25] samples, and the ESP adaptive sequential sampling method required only [13,24] samples. From the aspect of RMSE convergence trends, the ESP sampling strategy shows that there was a faster decline in prediction errors and smaller fluctuations than that of the LMD method.

The Pareto fronts attained by the ESP adaptive sequential sampling strategy during the iteration process for the two-objective functions (FONT) is compared with the real front, as shown in Fig. 13. It is obvious that the obtained Pareto fronts with RBF approximation can press close to the real front gradually as the sample points increase, although

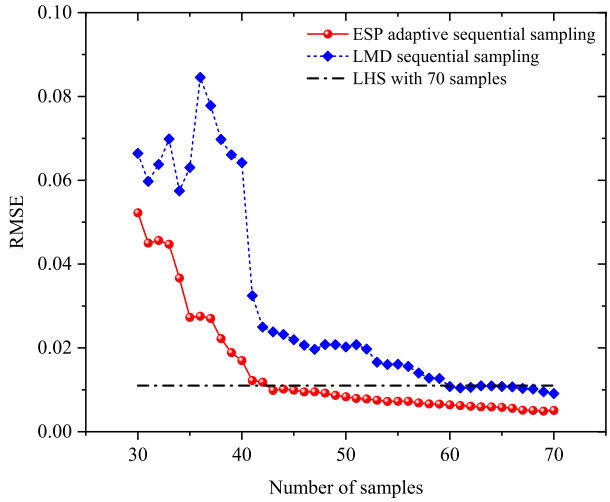

(a) RMSE convergence for F1.

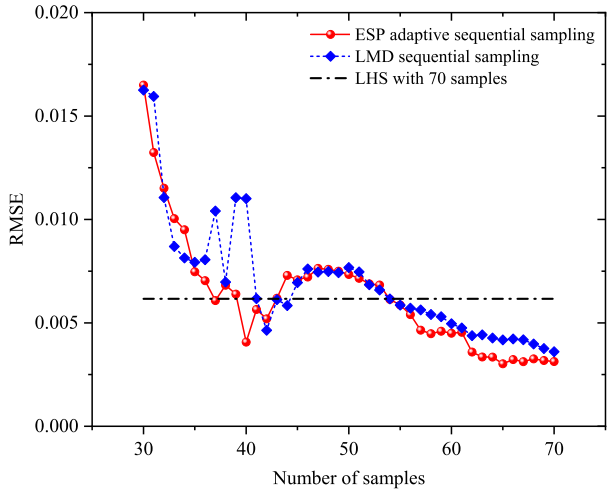

(b) RMSE convergence for F2.

FIGURE 12. RMSE convergence by different sampling methods.

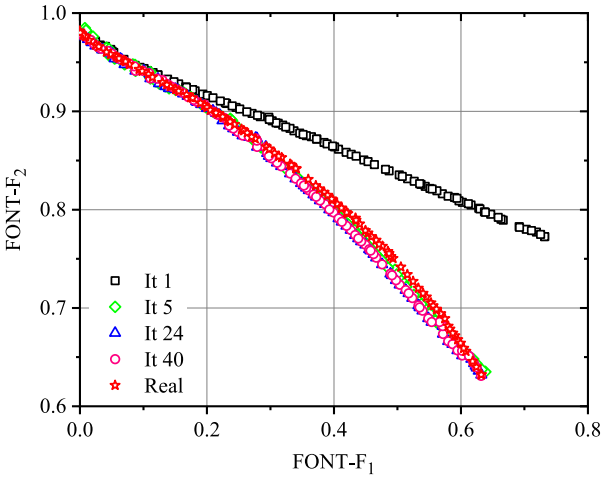

(a) Pareto fronts with RBF by ESP sampling.

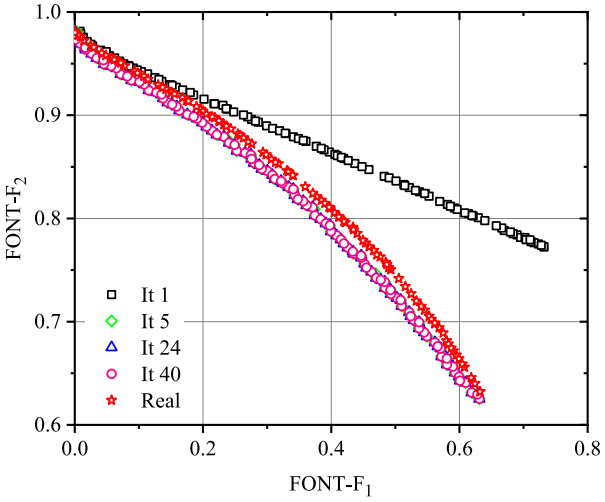

(b) Pareto fronts with RBF by LMD sampling.

FIGURE 13. Pareto fronts obtained by the ESP and LMD sequential sampling strategies compared with the real front.

the first several are revealed to be far away from the real front. Additionally, in order to quantitatively describe the astringency and distribution of the proximate Pareto fronts with the RBF meta model, the inverted generational distance performance index (IGD) [46] is applied in this paper, and can be expressed as follows

$$\mathrm{IGD}(P, Q) = \frac{\sum_{v \in P} d(v, Q)}{|P|} \tag{25}$$

where P and Q represent the point set evenly distributed along the real Pareto fronts and the Pareto optimal solution set obtained using RBF approximation respectively, and $d(v, Q)$ is the minimal Euclidean distance of the individual in the set P away from the population Q. Thus, it can be seen that the smaller value means the better combination property of the algorithm. The variation curves of IGD with different sequential sampling procedures in the test FONT are shown in Fig. 14. It was demonstrated that both IGD values were in a trend of decline as the sample points were reasonably increased. Moreover, the final values of the ESP sampling method achieved a stable level of less than 1% as the sequential sampling algorithm stopped, while the IGD values of LMD method achieved only 1.3%. The results suggest that the ESP sampling strategy performed excellently.

To sum up, the results of the tests highlighted that the adaptive ESP sequential sampling strategy proposed in this paper possesses the capability and the potential to improve the accuracy of the RBF surrogate model with a smaller sample size, which is used to replace real response values in respect of optimization variables during the search process. It was also effectively proved that the Pareto fronts obtained by applying RBF approximation to the multi-objective optimization can be very close to the real front. On the other hand, similar results of two different tests demonstrate that the proposed sampling method is suitable for many multi-objective optimization problems, and therefore has great prospects for applications in other scenarios.

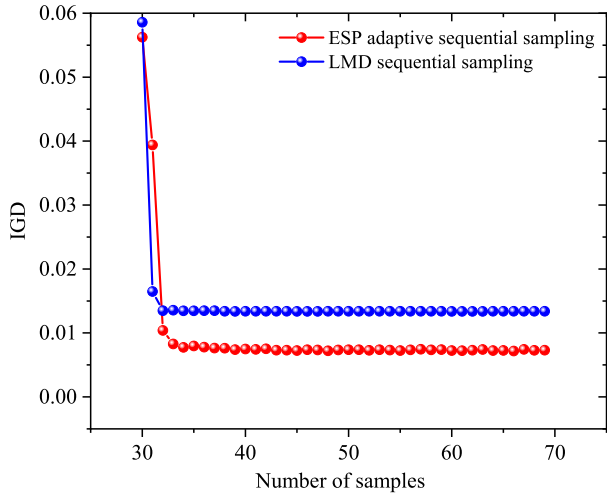

FIGURE 14. The variation curves of IGD by different sampling methods.

IV. THE ADAPTIVE ESP SEQUENTIAL SAMPLING FOR AERODYNAMIC OPTIMIZATION

A. OPTIMIZATION OBJECTIVES AND CONDITIONS

In this section, the proposed adaptive ESP sequential sampling method for aerodynamic optimization was implemented on a scaled model of the tandem-wing aircraft. In this application, we took $X = (S_t, G, r_b, \tau_1, \tau_2)^T$ as the design variables and regarded $Y = (C_L, K = C_L/C_{Di})^T$ as the objectives, where C_{Di} represented the induced drag calculated using non-planar VLM. It should be pointed out that the zero-lift drag coefficient was neglected, because the zero-lift coefficient is approximately invariable for different configurations with the same Reynolds number and viscosity coefficient in low speed flight conditions. Then, the following aerodynamic configuration optimization mathematical model can be constructed.

$$\begin{cases} Max: & [C_L(\alpha)]_{ascent} \\ & [K = C_L/C_{Di}]_{cruise} \\ st: & \alpha_{ascent} = 3^\circ \\ & C_{Lcruise} = 0.5 \\ & Area = constant \\ & H = 0\ m \end{cases} \tag{26}$$

B. OPTIMIZATION RESULTS AND DISCUSSION

- Case 1

Latin Hypercube and non-planar VLM were used to produce an initial database. Then, we carried out a comparison of the prediction accuracy of the three different surrogate models. The applicability of this method combined with the proposed ESP sampling method for strongly non-linear aerodynamic optimization was executed again. In this case, the initial database size was 30, and in view of computation cost for aerodynamic configuration optimization, the initial population and the maximal evolution number during the process of NSGA-II were set to 80 and 400, respectively.

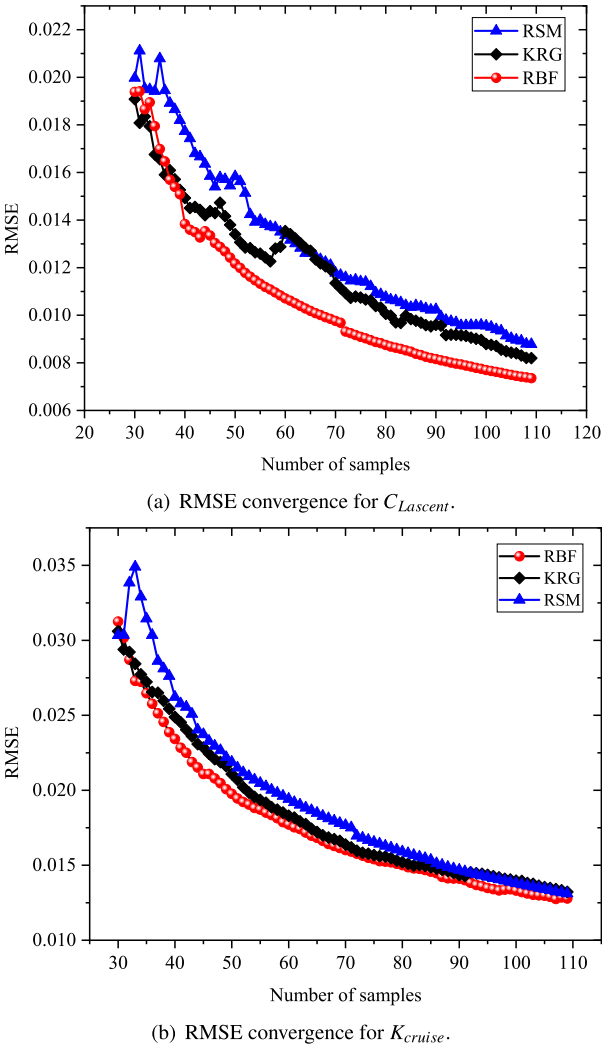

(a) RMSE convergence for $C_{Lascent}$.

(b) RMSE convergence for K_{cruise}.

FIGURE 15. RMSE convergence by different surrogate models.

The RMSE variation trends with a 80-step iteration are shown as Fig. 15.

According to the results, from the aspect of both accuracy and robustness, the capability of the RBF surrogate model to deal with the strongly non-linear problems was validated and sufficient to be considered superior to the other models.

- Case 2

Considering the influence of the initial sample points on the optimization, two different initial sample sizes, 30 and 40 samples with 6 and 8 times the number of design variables, were applied with the sequential sampling. Next, the adaptive sequential sampling was carried out after adding 80 samples to the initial database. The convergence process of RMSE for both objectives between RBF prediction and numerical approximation were recorded. In order to show the superiority of the proposed ESP adaptive sequential sampling strategy, a largest minimum distance (LMD) method was used as a contrast [47]. The comparison results are demonstrated in Fig. 16 and Fig. 17.

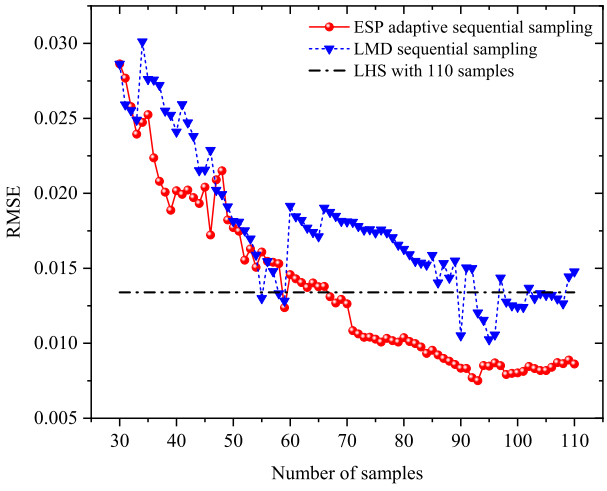

(a) RMSE for lifting coefficient C_L.

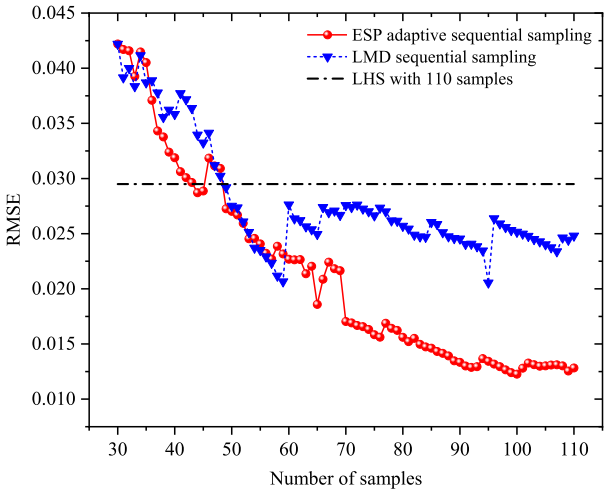

(b) RMSE for lift-drag ratio K.

FIGURE 16. RMSE convergence of two objective functions with 30 initial samples.

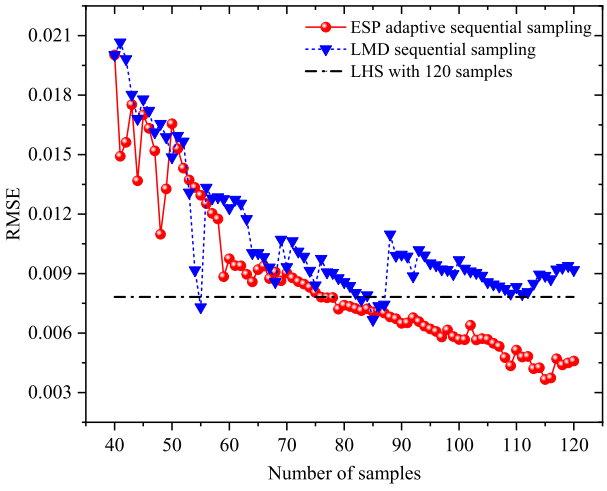

(a) RMSE for lifting coefficient C_L.

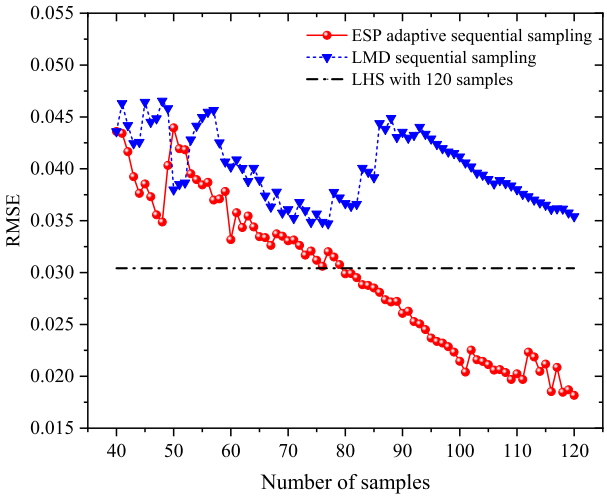

(b) RMSE for lift-drag ratio K.

FIGURE 17. RMSE convergence of two objective functions with 40 initial samples.

In Fig. 16, RMSE with 30 initial samples for lifting coefficient C_L and lift-drag ratio K decreases 69.9% and 69.6% respectively by using ESP adaptive sequential sampling, while the responding values are 48.4% and 41.2% when using LMD sequential sampling. Similarly, in the case whereby there are 40 initial samples, as shown in Fig. 17, the RMSE decrements of C_L and K reach 77.1% and 58.4% with ESP strategy, far exceeding the 54.1% and 18.8% reductions achieved with the LMD method. It appears to show that the precision of ESP adaptive sequential sampling was a significant improvement compared with the LMD method, especially for the lift-drag ratio K during flight cruises. Additionally, as the sample points increased, the precision of the two objectives steadily declined when using the ESP strategy, unlike the drastic fluctuation with the LDM method. Therefore, the efficiency of the database's refinement using ESP adaptive sequential sampling strategy was far better than the LMD method. Table 4 shows the added sample numbers needed to achieve the final accuracy (initial+80 samples) of the LMD method and the accuracy (initial+80 samples) of the LHS disposable sampling method respectively, by using the ESP strategy with different initial samples. Taking a case of 30 initial samples, in comparison with the LMD method and LHS method, ESP adaptive sequential sampling reduced the number of the numerical calculation more than 51 and 43 times, respectively, which signifies it would save time when running aerodynamic configuration optimization problems. Meanwhile, as we can see comprehensively in the two cases, the convergence process for both of the objectives was synchronous despite the difference in the initial sample sizes. Therefore, we verified that database refinement capabilities of the ESP adaptive sequential sampling strategy were insensitive to the initial sample size.

After 80 iterations of refinement, the Pareto fronts of each iteration based on NSGA-II were obtained by using the ESP adaptive sequential sampling strategy. Figure 18-19 show the variation process of the Pareto fronts at several typical steps with different initial sample sizes (30 and 40). It was

TABLE 4. The added sample numbers by using ESP strategy to get the accuracy by LMD and LHS sampling.

Objective	Initial samples size	Added samples size (LMD sampling)	Total samples size (LMD sampling)	Added samples size (LHS sampling)	Total samples size (LHS sampling)
lifting coefficient	30	29	59	37	67
$C_L(\alpha = 3°)$	40	27	67	37	77
lift-drag ratio	30	23	53	19	49
K_{cruise}	40	24	64	40	80

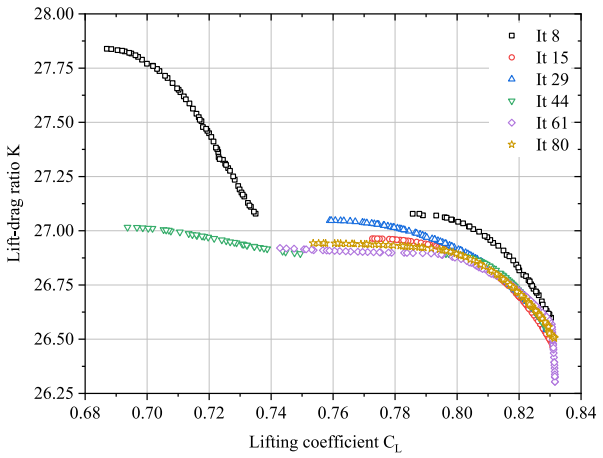

FIGURE 18. Pareto fronts of typical steps obtained by ESP with 30 initial samples.

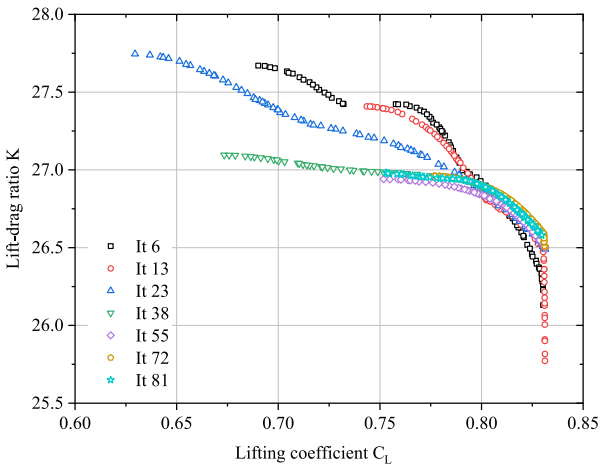

FIGURE 19. Pareto fronts of typical steps obtained by ESP with 40 initial samples.

indicated that when applying ESP adaptive sequential sampling strategy to enrich the database with refinement points, the Pareto front converges gradually to the final ones in two different initial sample size cases. Figure 20 shows the terminal Pareto fronts obtained using the ESP method with the two different initial sample sizes. It is clear that there was a negligible difference of no more than 0.3% on terminal Pareto fronts obtained with 30 and 40 initial samples, which further evidences the convergence of a multi-objective optimization strategy based on ESP adaptive sequential sampling and the credibility of optimization results.

On the other hand, as shown in Fig. 20, four typical design points (A,B,C,D) were picked out of terminal Pareto fronts in the case of 30 initial samples, to determine the optimal $C_{Lascent}$ and K_{cruise} with a clear conflict. Point A has the highest lift-drag ratio during the cruise compared with other points, while point D has the highest lifting coefficient at the ascent stage. Additionally, the performance of the initial layout of the tandem-wing UAV is used as a reference point ($C_L = 0.761$, $K = 24.157$) to help evaluate the optimal Pareto fronts. As a comparison, point B performs better in cruising but worse at the ascent than the reference point. Point C and points located in the dotted lines from point B to point D had good behavior during both two periods, which are the best choices for the aerodynamic configuration of the tandem-wing UAV. Point C was selected as the optimized layout, improving aerodynamic

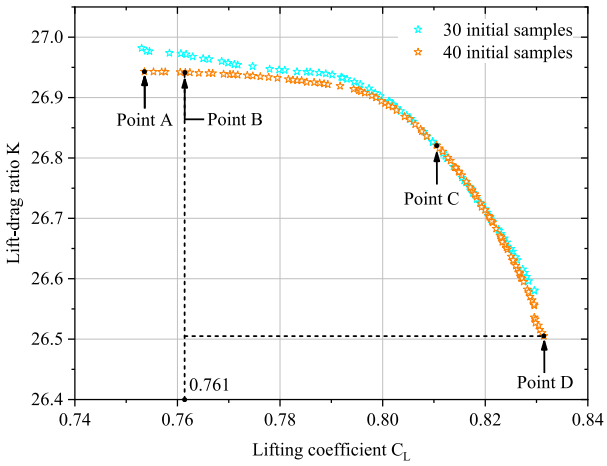

FIGURE 20. Terminal Pareto fronts obtained by ESP with different initial sample sizes.

characteristics of aircraft comprehensively. A quantitative performance comparison between the reference aerodynamic layout and optimized layout is shown in Table 5. It is presented that the $C_{Lascent}$ and K_{cruise} of the optimized layout improved 6.44% and 10.85% respectively, based on the non-planar VLM numerical calculation. Furthermore, Table 5 also shows that the only slight differences between RBF approximations and numerical calculation, narrowed to no more than 0.53% for both two objectives. Therefore, the

TABLE 5. Performance comparison of results between reference aerodynamic layout and optimized layout.

	RBF results		VLM results		Errors	
	$C_{Lascent}$	K_{cruise}	$C_{Lascent}$	K_{cruise}	$C_{Lascent}$	K_{cruise}
Reference layout	0.765	24.145	0.761	24.157	0.53%	0.05%
Optimized layout	0.811	26.821	0.810	26.778	0.12%	0.16%
Improvement	5.87%	11.08%	6.44%	10.85%	–	–

optimization results indicate that use of the ESP adaptive sequential sampling method is a reasonable multi-objective optimization strategy.

V. CONCLUSION

This study proposed an adaptive sequential sampling-based, multi-objective optimization process in order to optimize the aerodynamic configuration optimization of a tandem-wing UAV via a surrogate model. Considering the huge computational and time costs of the optimizing process when using non-planar VLM to consider two aerodynamic objectives, a surrogate model based on LOOCV was used to obtain the optimal shape parameter. To select the most advantageous surrogate model with the best predictive capabilities amongst the common alternative methods, a comparison based on indicators such as accuracy, robustness, and efficiency was developed. The result was that the RBF surrogate model had a superior and more comprehensive performance. In order to further decrease the size of the database without forsaking accuracy, an adaptive sequential sampling strategy taking into account the principle of entropy rank and a selection pooling method, was proposed for use the infilling criterion. In this way, the ability to search for global uncertainty regions and the ability to jump out of local optimal points were both guaranteed during the optimization process.

Three alternative surrogate models combined with ESP adaptive sequential sampling were engaged in two-objective optimization, validating the outstanding performance of the RBF surrogate model. On this basis, the integration of the RBF surrogate model and the ESP sampling strategy was explored and compared against LMD sampling and the disposable LHS method. The results demonstrated that the approximation errors of the RBF decreased sharply as the sequential sampling proceeded, greatly exceeding that with the same size of samples generated by previous methods. It was concluded that the ESP sampling strategy had the capability of saving calculation and time costs, and applicability. Besides, the Pareto fronts obtained during the sequential sampling procedure also got very close to the real fronts, highlighting the effectiveness of the ESP method. Consequently, these findings were applied to the tandem-wing UAV for the purpose of optimizing the aerodynamic configuration. Likewise, the RBF prediction accuracy of the aerodynamic characteristics to be optimized rose gradually as the sample points increased. Comparative research into LMD sampling and the LHS method showed that the prediction accuracy produced by the ESP sampling strategy was also more efficient. Meanwhile, it was explored whether the sizes of the initial sample database applied to the optimization had an impact on the results, and this revealed a synchronous trend, suggesting the insensitivity of the initial sample size to the sequential sampling. Eventually, compared with initial design aerodynamic layout of the tandem-wing UAV, the obtained Pareto fronts could be divided into two regions with three typical design points. A point producing a balance between the maximal $C_{Lascent}$ and maximal K_{cruise} was selected as the final optimal design point. The obvious improvement in the aerodynamic characteristics implied that the adaptive ESP sequential sampling optimization strategy could be applied during the preliminary design stages of aircrafts, in practical engineering.

This work was limited by the fact that the aerodynamic characteristics of the tandem-wing UAV were calculated using non-planar VLM, with which the numerical simulation precision is lower than high fidelity experimental and CFD methods. Therefore, further studies will be implemented by fabricating the prototype based on the optimized tandem-wing configuration, using the CFD method, and conducting experiments on aerodynamic characteristics to verify the feasibility.

ACKNOWLEDGMENT

The authors would like to thank the reviewers and editors for their very constructive comments, which have helped to improve the quality of this paper.

REFERENCES

[1] J. W. Bottomley, "The tandem-wing concept applied to modern transports," *Aeronaut. J.*, vol. 78, no. 767, pp. 523–524, 1974.

[2] R. Jones, D. J. Cleaver, and I. Gursul, "Aerodynamics of biplane and tandem wings at low Reynolds numbers," *Exp. Fluids*, vol. 56, no. 6, pp. 1–25, Jun. 2015.

[3] J. W. Bottomley, "Tandem wing aircraft," *Aerosp.-Basel*, vol. 4, pp. 12–20, Mar. 1977.

[4] T. Feistal, V. Corsiglia, and D. Levin, "Wind-tunnel measurements of wing-canard interference and a comparison with various theories," in *Proc. SAE Tech. Pap.*, Wichita, KS, USA, 1981, pp. 1–14.

[5] D. Fanjoy and D. Dorney, "A study of tandem-airfoil interaction in different flight regimes," in *Proc. 35th AIAA Aerosp. Sci. Meeting Exhibit*, Reno, NV, USA, Jan. 1997, pp. 1–18.

[6] V. K. Patidar, R. Yadav, and S. Joshi, "Numerical investigation of the effect of stagger on the aerodynamic characteristics of a Busemann biplane," *Aerosp. Sci. Technol.*, vol. 55, pp. 252–263, Aug. 2016.

[7] M. L. Rasmussen and D. E. Smith, "Lifting-line theory for arbitrarily shaped wings," *J. Aircr.*, vol. 36, no. 2, pp. 340–348, Mar. 1999.

[8] D. F. Scharpf and T. J. Mueller, "Experimental study of a low Reynolds number tandem airfoil configuration," *J. Aircr.*, vol. 29, no. 2, pp. 231–236, Mar. 1992.
[9] J. B. Fu, S. M. Ji, and X. Huang, "The effects of design parameters on tandem-airfoil configuration aerodynamics," in *Proc. 8th Asia–Pacific Int. Symp. Aerosp. Technol.*, Toyama, Japan, 2016, pp. 1–7.
[10] W. F. Phillips and D. O. Snyder, "Modern adaptation of Prandtl's classic lifting-line theory," *J. Aircr.*, vol. 37, no. 4, pp. 662–670, Jul. 2000.
[11] H. Cheng, Q. Shi, H. Wang, W. Shan, and T. Zeng, "Flight dynamics modeling and stability analysis of a tube-launched tandem wing aerial vehicle during the deploying process," *Proc. Inst. Mech. Eng., G, J. Aerosp. Eng.*, Apr. 2021, Art. no. 095441002110109, doi: 10.1177/09544100211010903.
[12] H. Cheng, H. Wang, Q. Shi, and M. Zhang, "Unsteady aerodynamics investigation of deploying tandem-wing with different methods," *Proc. Inst. Mech. Eng., G, J. Aerosp. Eng.*, vol. 233, no. 10, pp. 3714–3733, Aug. 2019.
[13] H. Cheng and H. Wang, "Prediction of lift coefficient for tandem wing configuration or multiple-lifting-surface system using Prandtl's lifting-line theory," *Int. J. Aerosp. Eng.*, vol. 2018, Jul. 2018, Art. no. 3104902, doi: 10.1155/2018/3104902.
[14] K. Deb, A. Pratap, S. Agarwal, and T. Meyarivan, "A fast and elitist multiobjective genetic algorithm: NSGA-II," *IEEE Trans. Evol. Comput.*, vol. 6, no. 2, pp. 182–197, Apr. 2002.
[15] R. P. Dwight and J. Brezillon, "Effect of approximations of the discrete adjoint on gradient-based optimization," *AIAA J.*, vol. 44, no. 12, pp. 3022–3031, Dec. 2006.
[16] J. Wild, "Multi-objective constrained optimisation in aerodynamic design of high-lift systems," *Int. J. Comput. Fluid Dyn.*, vol. 22, no. 3, pp. 153–168, Mar. 2008.
[17] J. Lee, K. Jung, and J. H. Kwon, "The aerodynamic shape optimization of airfoils using unconstrained trust region methods," *Eng. Optim.*, vol. 41, no. 5, pp. 459–471, May 2009.
[18] K. W. Lee, W. H. Moase, S. Z. Khong, A. Ooi, and C. Manzie, "Aerodynamic shape optimization via global extremum seeking," *IEEE Trans. Control Syst. Technol.*, vol. 23, no. 6, pp. 2336–2343, Nov. 2015.
[19] S. Qingli and W. Hua, "Inflatable airfoil structure optimization on flying wing buoyancy-lifting unmanned aerial vehicles," in *Proc. IEEE Int. Conf. Unmanned Syst. (ICUS)*, Beijing, China, Oct. 2017, pp. 254–259.
[20] C. Gong and B.-F. Ma, "Shape optimization and sensitivity analysis of a morphing-wing aircraft," *Int. J. Aeronaut. Space Sci.*, vol. 20, no. 1, pp. 57–69, Jan. 2019.
[21] I. Marinić-Kragić, D. Vučina, and Z. Milas, "3D shape optimization of fan vanes for multiple operating regimes subject to efficiency and noise-related excellence criteria and constraints," *Eng. Appl. Comput. Fluid Mech.*, vol. 10, no. 1, pp. 209–227, Feb. 2016.
[22] M. D. Manshadi and M. Jamalinasab, "Optimizing a two-element wing model with morphing flap by means of the response surface method," *Iranian J. Sci. Technol., Trans. Mech. Eng.*, vol. 41, no. 4, pp. 343–352, Dec. 2017.
[23] Y. Liang, X.-Q. Cheng, Z.-N. Li, and J.-W. Xiang, "Robust multi-objective wing design optimization via CFD approximation model," *Eng. Appl. Comput. Fluid Mech.*, vol. 5, no. 2, pp. 286–300, Jan. 2011.
[24] L. R. Zuhal, P. S. Palar, and K. Shimoyama, "A comparative study of multi-objective expected improvement for aerodynamic design," *Aerosp. Sci. Technol.*, vol. 91, pp. 548–560, Aug. 2019.
[25] X. Yan, J. Zhu, M. Kuang, and X. Wang, "Aerodynamic shape optimization using a novel optimizer based on machine learning techniques," *Aerosp. Sci. Technol.*, vol. 86, pp. 826–835, Mar. 2019.
[26] K. Ezhilsabareesh, S. H. Rhee, and A. Samad, "Shape optimization of a bidirectional impulse turbine via surrogate models," *Eng. Appl. Comput. Fluid Mech.*, vol. 12, no. 1, pp. 1–12, Jun. 2017.
[27] A. Diaz-Manriquez, G. Toscano-Pulido, and W. Gomez-Flores, "On the selection of surrogate models in evolutionary optimization algorithms," in *Proc. IEEE Congr. Evol. Comput. (CEC)*, New Orleans, LA, USA, Jun. 2011, pp. 2155–2162.
[28] T. J. Mackman, C. B. Allen, M. Ghoreyshi, and K. J. Badcock, "Comparison of adaptive sampling methods for generation of surrogate aerodynamic models," *AIAA J.*, vol. 51, no. 4, pp. 797–808, Apr. 2013.
[29] B. Zhang, Z. Feng, B. Xu, and T. Yang, "Efficient aerodynamic shape optimization of the hypersonic lifting body based on free form deformation technique," *IEEE Access*, vol. 7, pp. 147991–148003, 2019.
[30] W. Wang, Z. Wu, D. Wang, and W. Zhang, "Improved sequential approximate optimization for aerodynamic design benchmark problem," in *Proc. IEEE Congr. Evol. Comput. (CEC)*, Wellington, New Zealand, Jun. 2019, pp. 1110–1117.
[31] J. Huang, Z. Gao, Z. Zhou, and K. Zhao, "An improved adaptive sampling and experiment design method for aerodynamic optimization," *Chin. J. Aeronaut.*, vol. 28, no. 5, pp. 1391–1399, Oct. 2015.
[32] M. D. McKay, R. J. Beckham, and W. J. Conover, "A comparison of three methods for selecting values of input variables in the analysis of output from a computer code," *Technometrics*, vol. 42, no. 1, pp. 56–61, Feb. 2000.
[33] H.-S. Jeong and K.-Y. Kim, "Shape optimization of a feedback-channel fluidic oscillator," *Eng. Appl. Comput. Fluid Mech.*, vol. 12, no. 1, pp. 169–181, Oct. 2017.
[34] O. Ş. Gabor, A. Koreanschi, and R. M. Botez, "A new non-linear vortex lattice method: Applications to wing aerodynamic optimizations," *Chin. J. Aeronaut.*, vol. 29, no. 5, pp. 1178–1195, Oct. 2016.
[35] E. M. Cardenas, P. J. Boschetti, and A. Amerio, "Stability and flying qualities of an unmanned airplane using the vortex-lattice method," *J. Aircr.*, vol. 46, no. 4, pp. 1461–1464, Jul. 2009.
[36] J. Murua, R. Palacios, and J. M. R. Graham, "Applications of the unsteady vortex-lattice method in aircraft aeroelasticity and flight dynamics," *Prog. Aerosp. Sci.*, vol. 55, pp. 46–72, Nov. 2012.
[37] C. Xie, L. Wang, C. Yang, and Y. Liu, "Static aeroelastic analysis of very flexible wings based on non-planar vortex lattice method," *Chin. J. Aeronaut.*, vol. 26, no. 3, pp. 514–521, Jun. 2013.
[38] R. L. Hardy, "Multiquadric equations of topography and other irregular surfaces," *J. Geophys. Res.*, vol. 76, no. 8, pp. 1905–1915, Mar. 1971.
[39] J. Peter and M. Marcelet, "Comparison of surrogate models for turbomachinery design," *Wseas Trans. Fluid Mech.*, vol. 3, no. 1, pp. 10–17, Jan. 2008.
[40] J. Peter, M. Marcelet, S. Burguburu, and V. Pediroda, "Comparison of surrogate models for the actual global optimization of a 2D turbomachinery flow," in *Proc. 7th WSEAS Int. Conf. Simulation, Modelling Optim.*, Beijing, China, Sep. 2007, pp. 46–51.
[41] S. Rippa, "An algorithm for selecting a good value for the parameter c in radial basis function interpolation," *Adv. Comput. Math.*, vol. 11, no. 2, pp. 193–210, 1999.
[42] C. C. Xia, T. T. Jiang, and W. F. Chen, "Particle swarm optimization of aerodynamic shapes with nonuniform shape parameter–based radial basis function," *J. Aerosp. Eng.*, vol. 30, no. 3, pp. 1–12, May 2017.
[43] C. M. Fonseca and P. J. Fleming, "Multiobjective optimization and multiple constraint handling with evolutionary algorithms. II. Application example," *IEEE Trans. Syst., Man, Cybern., A, Syst. Humans*, vol. 28, no. 1, pp. 38–47, Jan. 1998.
[44] K. Deb, "Multi-objective optimization," in *Multi-Objective Optimization Using Evolutionary Algorithms*, 1st ed. New York, NY, USA: Wiley, 2001, ch. 2, pp. 13–48.
[45] K. C. Tan, T. H. Lee, and E. F. Khor, "Evolutionary algorithms with dynamic population size and local exploration for multiobjective optimization," *IEEE Trans. Evol. Comput.*, vol. 5, no. 6, pp. 565–588, Dec. 2001.
[46] D. A. Van Veldhuizen and G. B. Lamont, "On measuring multiobjective evolutionary algorithm performance," in *Proc. Congr. Evol. Comput. (CEC)*, La Jolla, CA, USA, Jul. 2000, pp. 204–211.
[47] S. Khalfallah and A. Ghenaiet, "Radial basis function-based shape optimization of centrifugal impeller using sequential sampling," *Proc. Inst. Mech. Eng., G, J. Aerosp. Eng.*, vol. 229, no. 4, pp. 648–665, Mar. 2015.

QINGLI SHI received the bachelor's degree in flight vehicle design from Beihang University, Beijing, China, in 2015, where he is currently pursuing the Ph.D. degree in flight vehicle design with School of Astronautics, under the supervision of Prof. Hua Wang. His research interests include the collective design of several unmanned aircraft vehicles, the aerodynamic layout design, and multi-objective optimization. He is currently researching the aerodynamic performances on the tandem-wing and the inflatable flying-wing buoyancy-lifting aircrafts.

HUA WANG received the Ph.D. degree from the Beijing Institute of Technology. His research interests include the new concept of micro small air vehicle technology, the design and analysis of the missile carried micro small aircraft systems, the design and analysis of the artillery lunched micro small aircraft systems, the effectiveness analysis of the weapon systems, and the fuze technology.

HAO CHENG received the M.S. and Ph.D. degrees from the School of Astronautics, Beihang University, Beijing, China, in 2014, and 2019, respectively. He is currently a Lecturer with the School of Astronautics, Beihang University. His research interests include new concept of micro small air vehicle technology, unmanned aerial vehicle design, and aerodynamic characteristics analysis on tandem-wing unmanned aerial vehicles, especially focusing on the study of unsteady aerodynamic characteristics near the status of stall.

FENG CHENG received the M.S. and Ph.D. degrees in flight vehicle system design from Beihang University, Beijing, China, in 2011 and 2018, respectively. He is currently an Engineer with the China Academy of Launch Vehicle Technology. His research interest includes flight vehicle structure design.

MENGLONG WANG received the M.S. and Ph.D. degrees in flight vehicle design from Beihang University, Beijing, China, in 2012 and 2018, respectively. He is currently an Engineer with the Beijing Electro-Mechanical Engineering Institute. His main research interest includes small aircraft design, flight control system design, and tactical missile design.